Morphology and Structure of Poly(di-*n*-butylsilane) Single Crystals Prepared by Controlling Kinetic Process of Solvent Evaporation

Zhijun Hu, Fajun Zhang, Haiying Huang, Minlu Zhang, and Tianbai He*

State Key Laboratory of Polymer Physics and Chemistry, Changchun Institute of Applied Chemistry, Chinese Academy of Sciences, Changchun 130022, China

Received July 6, 2003; Revised Manuscript Received February 24, 2004

ABSTRACT: The silicon backbone conformation in poly(di-*n*-butylsilane) (PDBS) has been shown to be a 7/3 helix at ambient conditions, which is in marked contrast to the near-planar conformation of its homologous polymers with side chain lengths of one to three or six to eight carbon atoms. In this work, both the 7/3 helical and near-planar chain conformations are achieved by controlling the solvent evaporation rate around room temperature. The chain conformation and crystal structure obtained in this method have been correlated to the crystal morphology by wide-angle X-ray diffraction, transmission electron microscopy, electron diffraction, optical microscopy, atomic force microscopy, and UV absorption spectrum. The lath-shaped single crystals obtained at 12 °C correspond to an orthorhombic form with near-planar chain conformation whereas the lozenge-shaped single crystals obtained at 30 °C (in coexistence with the lath-shaped crystals) are orthohexagonal with a 7/3 helix.

Introduction

Polysilane, an inorganic polymer with an all-silicon backbone, has been attracting considerable attention because of its unique electronic and optical properties.[1] Similar to those of π-conjugated polymers, it exhibits such semiconducting characteristics as photoconductivity,[2] charge carrier (holes) transport property,[3] and nonlinear optical effect,[4] due to the extensive delocalization of σ-electrons along the silicon backbone.

Many of the studies of polysilanes have focused on the symmetrically substituted poly(di-*n*-alkylsilane)s. Early studies[5−15] clearly revealed the relationships between side chain length, main chain conformation, phase structure, and electronic absorption band in the ordered crystalline phase. In polymers with side chain lengths of one to three and six to eight carbon atoms, the silicon backbone is historically identified with a near all-trans (or anti, A) conformation and the molecules arrange in an orthorhombic packing.[5−13] Contrarily, both poly(di-*n*-butylsilane) (PDBS)[14] and poly(di-*n*-pentylsilane) (PDPS)[5,9,14,15] were reported to adopt 7/3 helical chain conformation with an orthohexagonal packing under ambient conditions. These two distinct forms are associated with different UV absorption bands resulting from the $\sigma-\sigma^*$ interband transition.[16−18] The UV absorption spectrum of the helical form is typically centered near 315 nm, while the more planar conformation is typically centered at 375 nm.[18] Poly(di-*n*-alkylsilane)s with longer side chains have been found to have a four monomer AGAG′ repeat arranged in an orthorhombic packing and an intermediate UV absorption maximum near 335 nm.[17]

Molecular modeling calculations[19,20] showed that both the 7/3 helical and all-trans conformations were low-energy conformations for polysilanes, with the helical form being slightly lower in energy. Intermolecular interactions may be responsible for the near all-trans backbone conformation in the longer side chain homologues,[11] and a critical length of six carbon atoms is required to provide the necessary side chain interactions that would force the silicon backbone from its energetically preferred helical conformation into the near all-trans.[9] The adoption of near all-trans conformation in the shorter side chain polymers (methyl to propyl) has been attributed to more efficient packing of the molecules in the all-trans conformation than that would be possible for helical molecules.[6]

The more recent studies of symmetrically substituted poly(di-*n*-alkylsilane)s focused on the structural refinement and side chain packing motif. Oligosilane modeling studies[21,22] have identified a large number of thermodynamically stable intermediates (transoid (T), deviant (D), and ortho (O) with approximate Si−Si−Si−Si dihedral angles of 170°, 150°, and 90°, respectively) with the well-known all-trans, gauche (G), and helical backbone conformations.[22−25] Winokur and co-workers[26] also demonstrated that any silicon backbone in poly(di-*n*-alkylsilane)s historically identified with an all-trans conformation was not truly all-anti (or all-trans), but transoid and/or deviant structural conformers were presented.

Concerning the side chain packing motif, Patnaik and Farmer suggested[11] a symmetric tilted orientation of the alkyl side chains. In contrast to their result, recent studies[27−29] by Furakawa have proposed a highly asymmetric anti-syn packing of the alkyl side chains in which the hydrocarbon side chains are oriented nearly perpendicular to the Si backbone. Similarly, Winokur suggested[26] that the alkyl side chain construction can be closely identified as an asymmetric cisoid−transoid conformational arrangement.

In fact, polymorphism is quite common in conventional polymers, as an example of isotactic poly(1-butene). Three major crystalline forms, in which the polymer chains adopt different helical conformations and arrange in a crystal lattice with different symmetries, are obtained depending on the formation conditions.[30−33] The polymorphic behavior of isotactic poly(1-butene) is unique due to its solid state spontaneous transformation from the kinetically favored form II

* All correspondence should be addressed to this author. Telephone: +86-431-5262123. Fax: +86-431-5262126. E-mail: tbhe@ciac.jl.cn.

10.1021/ma034945n CCC: $27.50
Published on Web 03/31/2004

into the thermodynamically stable form I.[34] The important role of kinetics in conventional polymer phase transitions has been discussed and reviewed by Keller and Cheng.[35,36] Polymorphic behavior in σ-conjugated polysilanes and other π-conjugated polymers is distinctive because the structural forms have a profound impact on the resulting electronic and optical properties.[23] There are also prior reports of crystallographic polymorphism in symmetrically substituted poly(di-*n*-alkylsilane)s. Poly(di-*n*-alkylsilane)s with long alkyl substituents, such as poly(di-*n*-octylsilane) and poly(di-*n*-decylsilane), exhibit a diverse polymorphism with variable chain conformations, UV absorption spectra, and side chain packing motifs.[23,37,38] The studies of PDBS and PDPS have also indicated that the phase transition from the helical phase to the near-planar form is intrinsically possible based on the laws of thermodynamics. For example, Schilling et al. have found that a partial transformation of PDBS yielding stable trans sequences could be accomplished by application of pressure on the order of 50−500 MPa[39] or precipitation at very low temperatures (−78 °C).[40]

Therefore, the ability to control the crystallization process of poly(di-*n*-alkylsilane)s is critical in order to ensure that the correct polymorph is produced. One method is temperature-induced polymorphism as found in conventional polymers[35,36] and polydialkylsilanes.[23,38,40−42] In previous studies,[43,44] we showed that the solvent evaporation rate can kinetically control the microstructure of solution-cast block copolymer films. At fast or moderate solvent evaporation rate, a metastable phase (inverted phase) is kinetically frozen in, whereas the ultimate equilibrium state forms at an extremely slow rate. In this paper, we adopt the same approach to explore the polymorphism of PDBS under mild conditions by controlling the kinetics process of solvent evaporation.

In addition, although much progress has been made in the structural determination and refinement of symmetrically substituted poly(di-*n*-alkylsilane)s, less attention has been paid to correlating the crystal morphology with the structure. However, morphology plays a crucial role in the manipulation of physical properties of conjugated polymers and its knowledge is of utmost importance in any application.[45] Thus, understanding the relationship between structure, morphology, and properties remains a challenge in polysilanes.

In this study, we also attempt to correlate the crystal morphology with the structure of PDBS. Lath- and lozenge-shaped single crystals of PDBS with near-planar backbone conformation and 7/3 helical conformation, respectively, were obtained by controlling the evaporation of a toluene solution. The lath-shaped single crystals correspond to the orthorhombic form, whereas the lozenge-shaped single crystals (in coexistence with the lath-shaped crystals) are orthohexagonal.

Experimental Section

Materials. PDBS was prepared from the corresponding dichlorosilanes by dehalogenation coupling with sodium under standard conditions for polysilane synthesis by the Wurtz coupling reaction.[46] After purification from toluene with isopropyl alcohol (twice), a flocculent, pure white, oligomer-free sample of PDBS was obtained. The molecular weight determined by gel permeation chromatography (GPC) using polystyrene as the calibration standard in tetrahydrofuran solution was $M_n = 1.7 \times 10^4$ ($M_w/M_n = 1.8$).

Preparation of Single Crystals. PDBS powder sample was dissolved in toluene in a concentration of 0.1% w/v. A drop of solution was deposited onto carbon-coated mica, quartz plate, and silicon wafer, respectively. A slow solvent evaporation rate was achieved by placing the solution-cast films inside a cylinder container of radius and height 2.5 and 3.0 cm, respectively, covered with a lid. Toluene drops were placed around the substrate to generate a toluene partial pressure. Under these conditions, solvent can only escape through the small gap between the container and its lid. Since the vapor pressure of solvent varies with temperature, the solvent evaporation rate can be adjusted by varying temperature. In this experiment, the containers were maintained at 30 °C (vapor pressure of toluene 37 mmHg) and 12 °C (vapor pressure 14 mmHg), respectively. The evaporation of solvent in the solution was complete after approximately 5 and 10 h for the container maintained at 30 and 12 °C, respectively. After the solvent in the container also dried (ca. 1 and 3 days for the container maintained at 30 and 12 °C, respectively), the sample was taken out for observation.

Instruments. Wide-angle X-ray diffraction (WAXD) experiments were conducted with a Rigaku 18kw rotating-anode generator (Cu Kα) with a diffractometer as the detector with $I = 300$ mA and $V = 50$ kV. The X-ray beam was monochromized using a graphite crystal. The diffraction peak positions and widths were calibrated through silicon crystals with known crystal sizes. The 2θ angle region ranged between 3° and 40° with a scanning rate of 2.0°/min.

The macroscopic morphology of PDBS single crystals deposited on the surface of silicon wafer was observed via a Leica DMLP optical microscope. A light source in reflected mode was used to obtain the optical image.

The UV absorption spectra were obtained using a Cary 500 UV−vis−NIR spectrometer (Varian Analytical Instruments). Transmission spectra of the single crystals deposited on quartz were measured in the usual alignment (UV beam incidents normal to the surface). To obtain further information about the conformational and orientational states of the backbone, reflection spectra of single crystals deposited on silicon wafer were measured at different angles of incidence (the angle between the incident UV beam direction and the normal direction of the thin film) by automatically inclining the sample. The angle of incidence ranged from 20° to 70°. The spectra along with the schematic illustration are shown in Figure 9 and discussed in relation with the molecular orientation.

Transmission electronic microscopy (TEM) experiments were performed using a JEOL 2010 TEM with an accelerating voltage of 200 kV for bright field and electron diffraction (ED) modes. Before observation, the single crystals deposited on the carbon-coated mica were floated from the substrate in water and collected on a copper TEM grid. Platinum was evaporated on the sample for morphology observations. Calibration of the electron diffraction spacing was carried out using Au. A tilting stage was used in the ED experiments to determine the three-dimensional crystalline lattice.

The thickness and surface morphology of single crystals were investigated by atomic force microscopy (AFM) and friction force microcopy (FFM). The AFM and FFM experiments were performed with a SPA-300HV atomic force microscope (AFM) with an SPI 3800N controller (Seiko Instruments Industry Co., Ltd.). Pyramid-like Si_3N_4 tips, mounted on 100 μm triangle cantilevers with spring constants of 0.09 N/m, were applied for contact mode experiments of AFM and FFM. The FFM experiment was carried out according to the method described in ref 40 under a force of −0.02 nN (repulsive force). In the measurement of friction force by FFM, the long axis of the cantilever was perpendicular to the scanning direction, and then the degree of the cantilever torsion reflected precisely the magnitude of the friction force between the microtip and the sample surface. The scanning angle, θ, was varied from 0 to 90° by manually rotating the sample against the cantilever. The scanning angle, θ, was defined as the angle between the long axis direction of the lath-shaped single crystal, the {110} growth face of the lozenge-shaped

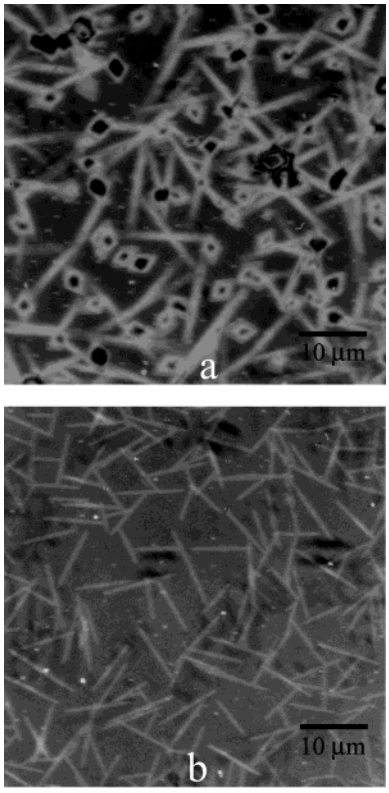

Figure 1. Reflective optical microscopy micrograph of PDBS samples: (a) crystallized at rapid solvent evaporation rate at 30 °C; (b) crystallized at an extremely slow rate at 12 °C.

single crystal, and the scanning direction (schematically illustrated in Figure 8a,b).

Results

Morphological Evolution Revealed by Optical Microscopy. In a previous study[48] we have shown that lamellar crystals with orthohexagonal intermolecular packing were obtained after dilute PDBS solution was spin-coated onto amorphous substrate. The lamellar crystals lack any anisotropy in dimensions due to the kinetically rapid process of crystallization.

However, when the solvent was slowly evaporated at 30 °C, PDBS was allowed to slowly crystallize during the solvent evaporation. Two polymorphs were clearly observed by optical microscopy (Figure 1a). One was lozenge-shaped lamellar crystals, and the other was lath-like lamellar crystals.

With further decrease of the temperature to 12 °C, the solvent evaporated at an extremely slow rate. As a result, PDBS molecules can crystallize at an extremely slow rate. Under this condition, only lath-like lamellar crystals were observed (Figure 1b).

It is known that the type of crystal habits formed is determined by the symmetry of the crystal unit cell.[49] A unit cell with lower rotational symmetry generates a more anisotropic crystal habit. On the other hand, polymers possessing higher rotational symmetry exhibit more isotropic polygonal lamellar habits. Since the anisotropy of lath-like lamellar crystals is higher than that of the lozenge-shaped lamellar crystals, it is reasonable to estimate that the rotational symmetry of the crystal unit cell of the former is lower than that of the latter.

Structural Transition Determined by WAXD. To investigate the influences of solvent evaporation rate on the crystal structures, the nascent PDBS sample precipitated from toluene with isopropyl alcohol was first studied by X-ray diffraction, as shown in Figure 2. The diffraction pattern was similar to that obtained from the high molecular weight sample.[14] It was dominated by a strong reflection centered at 8.32° 2θ, which corresponded to the (110) and (020) reflections in the orthohexagonal packing with 7/3 helical chain conformation.[14] The three weak peaks in the 19°−22° 2θ range have both inter- and intramolecualr components. The paucity of diffraction peaks compared with the rich pattern in poly(di-*n*-hexylsilane)[13] indicated the more poorly ordered crystalline structure for the PDBS sample. However, the orthohexagonal phase was not perfectly pure. As seen in the lower part of Figure 2, the peak centered at 8.32° contains two distinct shoulders. The composite peak can be deconvoluted into three Lorentzians centered at 7.96°, 8.32°, and 8.91° (1.11, 1.06, and 0.99 nm, respectively), similar to that observed in ref 14. The peak at 7.96° can be indexed as the (020) reflection in the near-planar phase of PDBS obtained under higher pressure.[26] However, the reflection at 8.91° has not been indexed so far. It is likely to result from a more complicated phase. Nevertheless, the above results indicated that a small quantity of two or more distinct structures coexisted in the nascent sample. Similar phenomena have been found in the high molecular weight PDBS sample[14] and low molecular weight PDPS sample.[41]

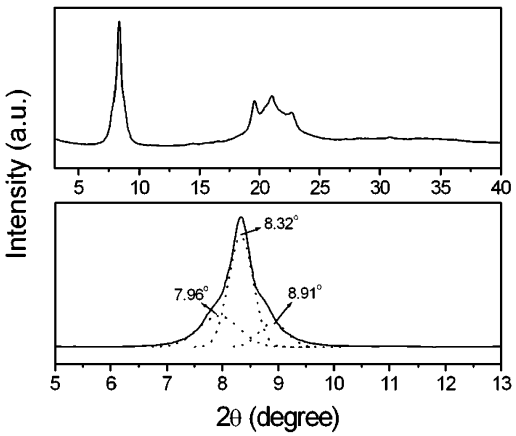

Figure 2. X-ray diffractions of nascent PDBS sample.

Upon the solvent being slowly evaporated at 30 °C, besides the reflection at 7.96° two additional reflections at 9.47° and 18.06° 2θ (0.93 and 0.49 nm, respectively) became apparent, as shown in Figure 3b. (To compare conveniently, the WAXD curve of the nascent sample is also included as Figure 3a.) The increase in the number of reflections compared to the nascent sample implied a much more regular interchain packing than the 7/3 helical phase. The transformation of interchain packing in PDBS induced by solvent evaporation was similar to that induced by external pressure.[39] The crystallographic changes in the sample can be attributed to a partial conversion of PDBS from the orthohexagonal structure with 7/3 helical chain conformation to a more ordered packing with near-planar chain conformation, accompanied by a large increase in three-dimensional order.[39] However, the reflection at 8.32° 2θ, corresponding to the (110) and (020) reflections in the orthohexagonal packing, still remained prominent. The reservation of interchain packing of the 7/3 helical conformation indicated that the transformation was not complete

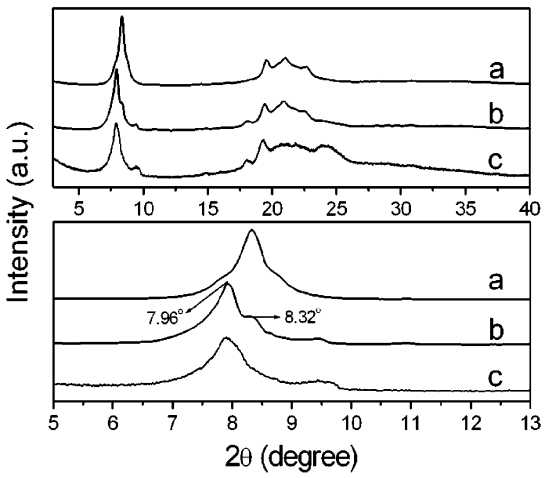

Figure 3. X-ray diffractions of PDBS crystals prepared by various methods: (a) nascent sample precipitated from toluene at room temperature; (b) sample crystallized at slow solvent evaporation rate at 30 °C; (c) sample crystallized at an extremely slow rate at 12 °C.

and both crystalline phases coexisted in this case. As a result, two polymorphs are observed under optical microscopy (Figure 1a).

With further decrease of the solvent evaporation rate, the diffraction peak (Figure 3c) corresponding to the orthohexagonal packing observed in Figure 3a,b completely disappeared and only the diffraction peaks corresponding to the near-planar form was observed, indicating the 7/3 helical phase entirely transformed to the more ordered crystalline form with near-planar chain conformation. The preservation of lath-like lamellae (Figure 1b) may indicate that the silicon backbone of PDBS in the lath-like lamellae adopt a near-planar conformation. Accordingly, the silicon backbone in the lozenge-shaped lamellar crystals obtained at the extremely slow solvent evaporation rate at 30 °C adopts the 7/3 helical conformation.

Single Crystal Structures Determined by TEM. TEM indicated that both kinds of PDBS crystals obtained here were single crystals. Figure 4 shows the typical TEM image and corresponding ED pattern of the lozenge-shaped lamellar single crystal. The aspect ratio between the two axes of the lozenge-shaped single crystal is 1:1.6, and the angles between the growth faces are 64° and 116°. In addition, the lozenge-shaped lamellar single crystal shows striations at right angles to the {110} growth faces, highlighting a sectorization of crystals with the two diagonals as boundaries. This kind of corrugation has been described for some polyesters[50] and nylons[51] and interpreted as a consequence of a chain axis shift between neighboring chains along the growing planes.

As shown above, the silicon backbone in the lozenge-shaped single crystal is 7/3 helix and the solid-state structure of the single crystal is orthohexagonal packing. The corresponding ED pattern contains six independent diffraction spots at 1.07 nm, which correspond to the 020 and 110 diffraction in the orthohexagonal packing of the 7/3 helical silicon chains in PDBS.[14] We noted that the intensity of the electron diffraction along the long diagonal direction of the crystal was weaker than that of the other four diffraction spots. Therefore, it is reasonable to index the two relative weak diffraction spots along the long diagonal direction of the crystal as 020 and the other four spots as 110 in terms of

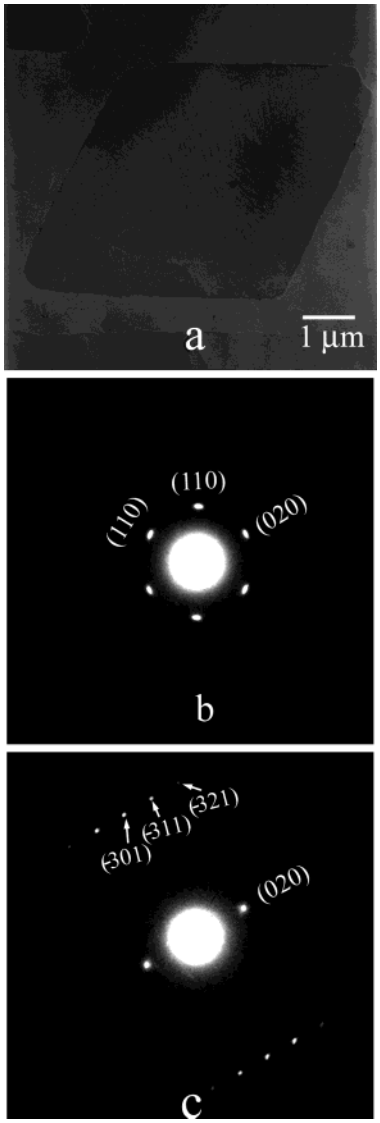

Figure 4. (a) Bright field electron microscopy image of a PDBS lozenge-shaped single crystal obtained at a slow solvent evaporation rate at 30 °C. (b) Electron diffraction pattern of the single crystal with a proper crystallographic orientation. (c) An ~16°-tilted ED pattern around the *b* axis.

orthohexagonal lattice parameters $a = 1.25$ and $b = 2.14$ nm. These parameters are in agreement with a unit cell containing two chain segments and a cross-sectional area per chain of 1.34 nm^2. These parameters are slightly smaller than those Schilling reported[14] previously ($a = 1.284$, $b = 2.224$ nm) on the basis of an X-ray fiber diagram. This may be due to the breadth of reflection in the X-ray fiber diagram. Thus, the lozenge-shaped single crystal could be considered to occur with {110} as growth planes, like a lozenge-shaped polyethylene lamellar single crystal.[52]

The three-dimensional structure was determined by a base-plane electron diffractogram combined with the diagrams tilted around the crystallographic *b* axis. When the single crystal was tilted by about 16° around the *b* axis, the 110 diffraction completely disappeared as shown in Figure 4c. One sees a series of ($-3k1$) spots -301, -311, and -321 at 0.425, 0.414, and 0.388 nm, respectively. From this, the *c* dimension of the unit cell was determined to be 1.39 nm, which was consistent with what Schilling et al. reported[14] previously based on an X-ray fiber diagram. Therefore, the basic ortho-

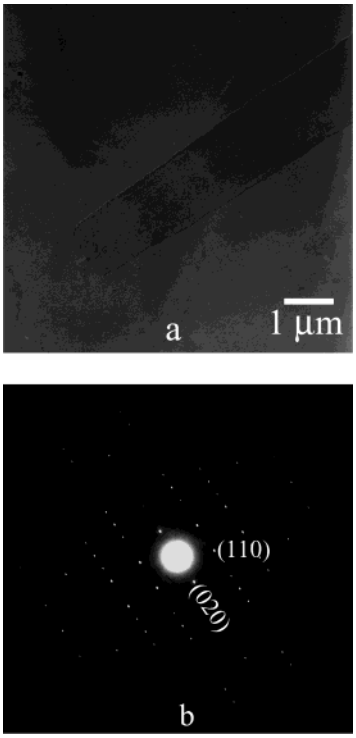

Figure 5. (a) Bright field electron microscopy image of a PDBS lath-shaped single crystal obtained at an extremely slow rate at 12 °C. (b) Electron diffraction pattern of the single crystal with a proper crystallographic orientation.

hexagonal unit cell structure has $a = 1.25$ nm, $b = 2.14$ m, and $c = 1.39$ nm. The TEM results are consistent with those by WAXD and optical microscopy.

Figure 5 shows the TEM image and ED pattern of a highly faceted, regular, lath-shaped lamellar single crystal with extremely slow solvent evaporation rate at 12 °C. The single crystal yielded a sharp electron diffraction diagram which contained more than 60 independent reflections that were mirrored in the four quadrants, which indicated a higher ordered structure in the lath-shaped single crystal than that in the lozenge-shaped lamellar single crystal. The ED pattern has a close resemblance to that of the flat-on lamellae of PDHS.[48] According to the WAXD results[26] of PDBS with near-planar type phase obtained at higher pressure, it is apparent that all the diffraction spots correspond to *hk*0 diffraction. The [001] zonal ED pattern suggests that the lath-shaped single crystal grows as a flat-on type with the molecular chain (i.e., *c* axis) perpendicular to the growing substrate. In this way, all the observed sharp reflections could be indexed according to an orthorhombic lattice of $a = 1.03$ and $b = 2.22$ nm, with 020 (1.11 nm) and 110 (0.94 nm) being the most intense ones. Accordingly, the reflection at 18.06° 2θ in WAXD can be indexed as (210). These parameters were consistent with the structural model with an anti backbone conformation and an asymmetric cisoid−transoid side chain arrangement proposed by Winkokur.[26] The calculated cross-sectional area per chain is 1.14 nm^2.

The ED patterns in Figure 5b also indicated that the growth faces of the lath-shaped single crystal corresponded to the {100} and {010} planes and the crystallographic *a* axis was parallel to the long axis of the lath-shaped single crystals.

Theoretically, the three-dimensional structure of the lath-shaped single crystal can also be determined by a base-plane electron diffractogram combined with the diagrams tilted around crystallographic *a* or *b* axis. Unfortunately, the tilt limit of our TEM is ±30°. Within this range, no other diffraction spots were observed. Therefore, the *c*-axis dimension of the lattice was not indexed.

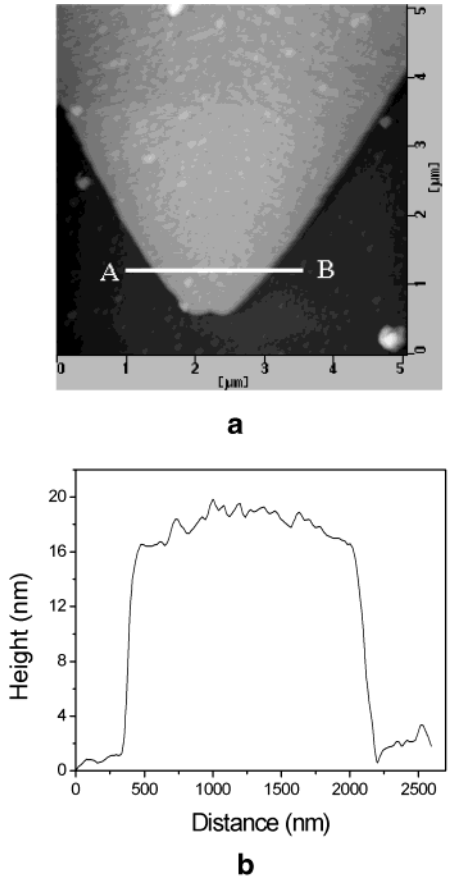

Figure 6. (a) AFM height image of a PDBS lozenge-shaped single crystal. (b) The profile line of the cross section between A and B shown in (a).

Nevertheless, the rotational symmetry of the orthorhombic unit cell of the lath-shaped single crystals is lower than that of the lozenge-shaped ones. Therefore, the more anisotropic single crystal habits formed for PDBS with an orthorhombic unit cell.

Chain-Folding Structure at the Single Crystal Surfaces. It is well-known that polyethylene[50,53,54] and polypropylene[55] single crystals have chain folding at lamellar surfaces. The measurement of lamellar thickness and surface friction property by atomic force microscopy is a quite useful technique for elucidating the chain-folding structure of lamellar single crystals and the chain-folding direction on the crystal surface.[47]

The thickness of the lozenge-shaped lamellar single crystal was measured by AFM to be about 16−20 nm (shown in Figure 6). Taking into account the repeat distance of 1.39 nm and molecular weights, the chain folding occurred at the surface of the lozenge-shaped lamellar single crystal with an appropriate conformational change like those in the lozenge-shaped polyethylene single crystals.[50,53] The thickness of the lath-shaped single crystals was about 7.5−9 nm (Figure 7). Although multilayer morphologies were observed for the lath-shaped single crystal, the thickness of each layer was close to 8 nm. Therefore, the chain folding also occurred at the surface of lath-shaped lamellar single crystal.

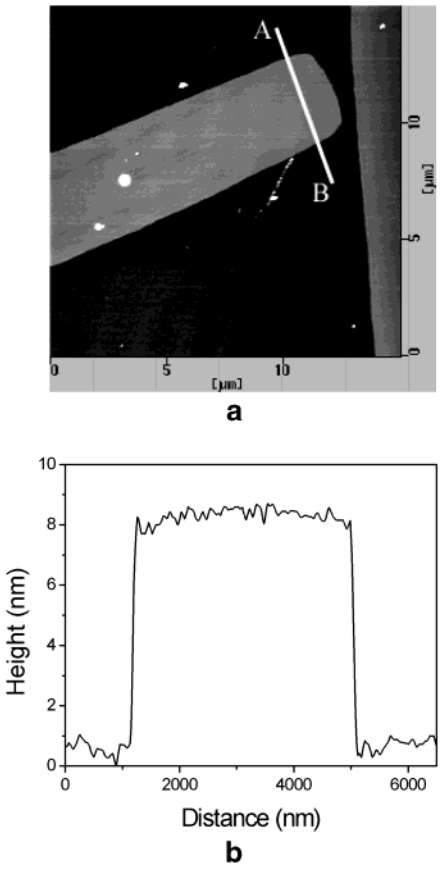

Figure 7. (a) AFM height image of a PDBS lath-shaped single crystal. (b) The profile line of the cross section between A and B shown in (a).

Obviously, the lamellar thickness of lozenge-shaped single crystal (16−20 nm) was markedly larger than that of the lath-shaped single crystal (7.5−9 nm). It has been reported that a single crystal tended to grow two-dimensionally, i.e., through lateral growth and thickening growth, because the thermodynamic driving force and the sliding diffusion of chains within the single crystal played essential roles.[56] The thickening growth of a single crystal depended on chain packing density. The looser the chain packing is, the easier the thickening growth is. According to the above discussion, the cross-sectional area per chain of PDBS lozenge-shaped single crystal was much larger than that of lath-shaped single crystal; i.e., the cell density of the former was much smaller and the chain packing was much looser than that of the latter. Therefore, the thickening growth rate of lozenge-shaped single crystal was larger and the sliding diffusion of chains occurred easily.

The FFM experiment was performed to reveal the regularity of chain folding on the surface of the two kinds of lamellar single crystals, which reflects the tribological properties and structural symmetry at the surface.[57] The FFM observation of polyethylene lozenge-shaped single crystals was reported by Kajiyama et al.[47] Depending on the scanning direction of the cantilever tip, it might experience lower friction when the tip is slid along folding loops or higher friction when the tip is bumped into the folding loops.[57] In our FFM measurements, the definition of the scanning angle, θ, is shown in parts a and b of Figure 8 for the lozenge-shaped and lath-shaped lamellar single crystals, respectively. Figure 8c shows the scanning angle dependence of the friction force for lozenge- and lath-shaped

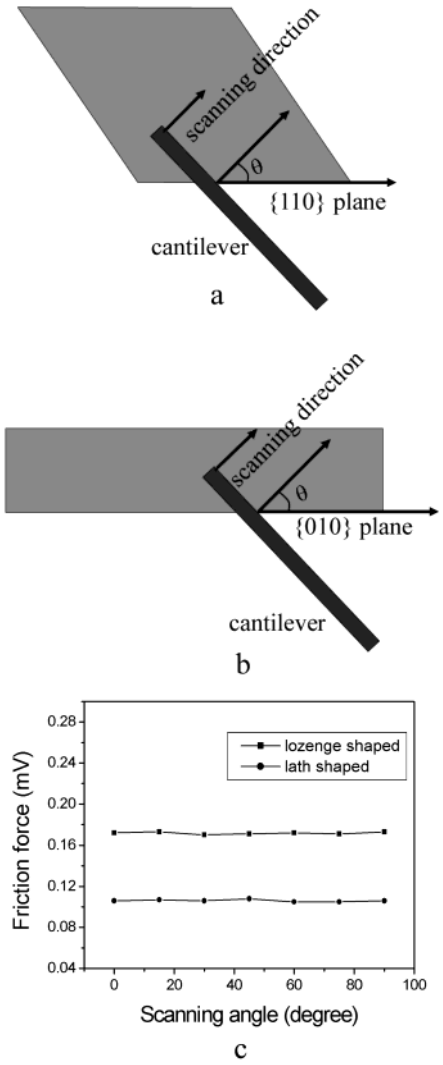

Figure 8. (a) Schematic representation of the definition of the scanning angle, θ, of lozenge-shaped lamellar single crystal. (b) Schematic representation of the definition of the scanning angle of lath-shaped lamellar single crystal, in the friction force measurement. (c) Scanning angle dependence of the friction force for both kinds of PDBS single crystals.

lamellar single crystals. It can be clearly seen that the magnitude of the friction force for both crystals is independent of the scanning angle, θ. The result indicates that a regular direction of the chain folding is not present at the surface of the two kinds of single crystals. The phenomenon was also observed in the lozenge-shaped single crystal of polyethylene with a high molecular weight,[47] in which sectored striations were observed. Therefore, it was reasonable to conclude that there was an amorphous layer on the top of the crystal stems of both single crystals. In addition, the magnitude of the friction force was larger for the lozenge-shaped lamellar single crystal than that for the lath-shaped single crystal. This was due to the higher roughness at the surface of the lozenge-shaped lamellar single crystal.

Silicon Backbone Conformation and Orientation in Lath-Shaped Single Crystals. UV absorption spectral measurements provide useful information on both the conformational and orientational states of the backbone due to the delocalization of the σ-electrons along the catenated silicon chain.[58,59] Since the silicon backbones in the lath-shaped single crystals adopt a near-planar conformation, a UV absorption maximum

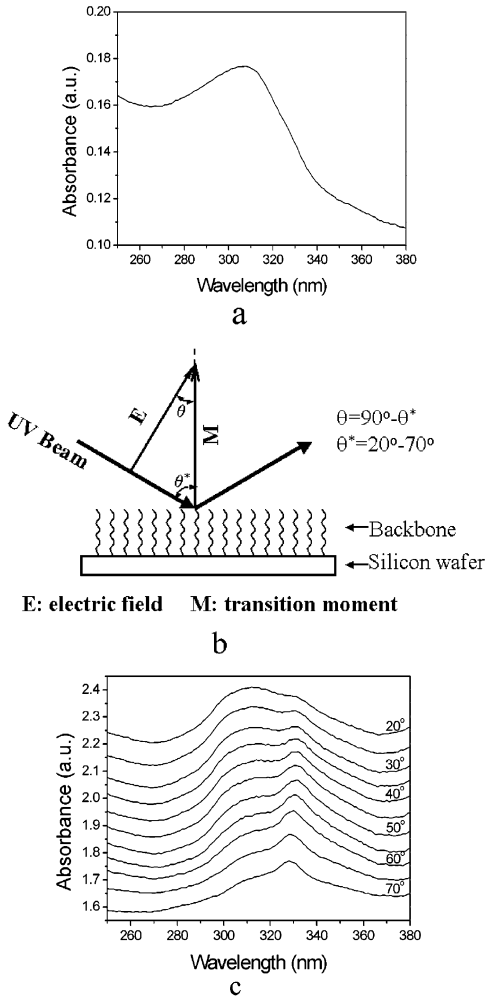

Figure 9. (a) UV absorption spectra of PDBS lath-shaped crystals measured in transmission mode. (b) Schematic illustration of the relation between UV incident beam and structure of PDBS lamellae with silicon backbone parallel to the surface of substrate. (c) UV absorption spectra of PDBS lath-shaped lamellae deposited on the surface of silicon wafer at various θ^* angles between incident UV beam direction and direction normal to the thin film.

should be observed at wavelengths longer than the helical form. Figure 9a shows the ordinary UV absorption spectrum of PDBS single crystals on quartz prepared with extremely slow solvent evaporation rate at 12 °C. Interestingly, only one absorption maximum at 307 nm corresponding to the 7/3 helix or disordered form was observed. It seemed that only the 7/3 helix or disordered form was taken for the PDBS backbone in the lath-like lamellar crystals, which contradicted the results of WAXD, TEM, and optical microscopy. However, we noted that the UV absorption spectrum shown in Figure 4a was performed in transmission mode with UV beam incidents normal to the surface. According to the principle of optical absorption,[60] the UV absorbance is proportional to $M^2E^2\cos^2\theta$, where M is the transition moment of conjugated molecule, E is the electric field of incident UV beam, and θ is the angle between the electric field and transition moment. Since UV absorptions of polysilanes are generally attributed to the σ-electron delocalization along the main chains, no absorption should occur with the normal incident beam if the main chains align perpendicular to the substrate (Figure 9a).

With the inclined-sample alignment, however, absorption due to the main chains can be observed (Figure 9b,c), because the main chains are not perpendicular to the electric field of the incident beam. In this work, reflection UV absorption measurements were carried out for the lath-shaped single crystals deposited on silicon wafer by varying the angle of incidence, θ^* (the angle between the incident UV beam direction and the normal direction of the substrate). If the silicon backbone of PDBS lath-shaped lamellar crystals is perpendicular to the surface of substrate, the angle θ between the electric field of the incident UV beam and the transition moment of silicon backbone is equal to $90° - \theta^*$, i.e., $\theta = 90° - \theta^*$ (schematically illustrated in Figure 9b). Figure 9c shows the UV absorption spectra of PDBS lath-like lamellar crystals at different angles of θ^*. A strong absorbance at 307 nm accompanied by one weak absorption peak at ca. 330 nm was observed at $\theta^* = 20°$. On one hand, the absorption peak around 330 nm was already observed for PDBS precipitated at low temperature (Figure 2b in ref 40), where it was attributed to the disordered conformational component of the polymer. On the other hand, this absorption peak was also observed in symmetrically substituted poly(di-*n*-alkylsilane)s with shorter side chains (poly(dimethylsilane),[7] poly(diethylsilane),[8] and poly(di-*n*-propylsilane)[8]), where near all-trans conformations have been historically documented, and unsymmetrically substituted poly(di-*n*-alkylsilane)s.[18] However, in the well-ordered crystalline phase of poly(di-*n*-hexylsilane) that truly approximates a trans-planar conformation of the backbone, the UV absorption peak is around 370 nm. Hence the silicon backbone of lath-shaped single crystals must contain a large proportion of transoid, deviant, or ortho conformations. For PDBS under higher pressure, Winokur et al. suggested[26] the actual model roughly approximates a TTTD-type repeat structure. Similarly, crystalline poly[(methyl-*n*-hexyl)silane], which exhibits a UV absorption around 330 nm, also incorporates a D/T-based Si backbone and locally approximates a D + T + D − T motif.[18] This indicated the presence of significant nonplanarity in the form of transoid and/or deviant structural conformers. Therefore, we call this more planar conformation a near-planar one.

Moreover, the UV absorption spectra shown in Figure 9c indicate stronger absorption at 330 nm at a larger θ^* angle. That not only proves that the silicon backbone in the stems of lath-like lamellar crystals take a near-planar conformation, but also indicate the silicon backbone is perpendicular to the basal plane.

It should be pointed out that the observation of the broad absorption peak at 307 nm predicted the existence of 7/3 helix or disordered form in the lath-like lamellar crystal. Since no deflection corresponding to orthohexagonal packing of 7/3 helical backbone was observed in the X-ray diffraction of lath-like lamellar crystals shown in Figure 3c, the broad absorption peak at 307 nm must correlate to the disordered form. The FFM results show that there was an amorphous layer on the top of the crystal stems, which may contribute to the broadening of the absorption peak at 307 nm. On the other hand, there may be an amorphous layer surrounding the single crystals, similar to isotactic polystyrene crystallized in thin films.[61]

Discussion

It is not entirely surprising that both the 7/3 helical and near-planar chain conformation were obtained at

the slow solvent evaporation rate. Molecular modeling calculations,[19,20] which considered only intramolecular interactions, showed that both the 7/3 helical and all-trans conformations were low-energy conformations for the silicon backbone of polysilanes, with the helical form being slightly lower in energy. This suggests that it is possible for the silicon backbone of PDBS to adopt either the 7/3 helical or near-planar conformation in the solid state. However, the net influence of the side chain in PSBS is more pronounced due to the unimportance of side chain crystallization.[14] As a result, helical chain conformation was frequently observed for PBBS. On the other hand, the near-planar molecules pack more efficiently than the helical molecules (as in the symmetrically substituted poly(di-*n*-alkylsilane)s with shorter side chains),[6] thus leading to a more closed packing mode. This suggests that the near-planar packing of PDBS molecules is a thermodynamically stable state and 7/3 helical packing is a thermodynamically metastable state. Although the metastability is determined by thermodynamics, in the majority of cases of phase transitions the metastable state is practically determined by the kinetics.[35] A metastable state may exist due to its fast kinetic pathway during a transformation process even though this state is thermodynamically less stable than the equilibrium state. Winokur and coworkers also suggested[23] that at least two distinct molecular level ordering mechanisms, intrachain and interchain, are present for the polymorphism of poly(di-*n*-alkylsilane)s with longer side chains. The intrachain ordering processes proceed with relatively rapid time scales while the interchain ordering can require substantially longer times. Therefore, during the fast crystallization from solution, the PDBS molecules have a larger probability to choose a pathway which possesses a lower energy barrier regardless of the thermodynamic stability after the barrier is overcome. Nevertheless, when the solvent is evaporated at an extremely slow rate at 12 °C, the PDBS molecules have enough time to diffuse over a distance, remove volatile solvent, exclude defects or otherwise optimize the chain packing in the crystalline regions, and maximize the probability of achieving the thermodynamic equilibrium state. This is similar to increasing the temperature during crystallization from isotropic melt. Thus, only the stable state with near-planar chain conformation was obtained when the solvent was evaporated at an extremely slow rate at 12 °C.

Conclusion

It was previously found that PDBS adopts a 7/3 helical rather than a near-planar conformation at ambient conditions. The near-planar conformation was observed only under extreme conditions. However, by controlling the solvent evaporation rate, we were able to control the polymorphs of PDBS crystals around room temperature. At relatively high solvent evaporation rate, both lozenge-shaped and lath-shaped single crystals exist. At extremely low rate, however, only the lath-shaped single crystal is found. The lath-shaped single crystals correspond to the orthorhombic form with near-planar chain conformation whereas the lozenge-shaped single crystals are orthohexagonal with 7/3 helical chain conformation. A mechanism based on kinetic effects was proposed to explain the origin for the formation of polymorphism.

Acknowledgment. The authors thank Prof. Stephen Z. D. Cheng at the Institute of Polymer Science of the University of Akron for helpful discussions. This work was supported by the National Science Foundation of China.

References and Notes

(1) Miller, R. D.; Michl, J. *Chem. Rev.* **1989**, *89*, 1359.
(2) Harrah, L. A.; Zeigler, J. M. *J. Polym. Sci., Polym. Lett.* **1985**, *23*, 309.
(3) Dewar, M. J. S. *J. Am. Chem. Soc.* **1984**, *106*, 669.
(4) Hasegawa, T.; Iwasa, Y.; Kishida, H.; Koda, T.; Tokura, Y.; Tachibana, H.; Kawabata, Y. *Phys. Rev. B* **1992**, *45*, 6317.
(5) Karikari, E. K.; Greso, A. J.; Farmer, B. L.; Miller, R. D.; Rabolt, J. F. *Macromolecules* **1993**, *26*, 3937.
(6) Patnaik, S. S.; Farmer, B. L. *Polymer* **1992**, *33*, 5121.
(7) Lovinger, A. J.; Davis, D. D.; Schilling, F. C.; Padden, F. J.; Bovey, F. A.; Zeigler, J. M. *Macromolecules* **1991**, *24*, 132.
(8) Lovinger, A. J.; Davis, D. D.; Schilling, F. C.; Bovey, F. A.; Zeigler, J. M. *Polym. Commun.* **1989**, *30*, 356.
(9) Farmer, B. L.; Rabolt, J. F.; Miller, R. D. *Macromolecules* **1987**, *20*, 1167.
(10) Rabolt, J. F.; Hofer, D.; Miller, R. D.; Fickes, G. N. *Macromolecules* **1986**, *19*, 611.
(11) Patnaik, S. S.; Farmer, B. L. *Polymer* **1992**, *33*, 4443.
(12) Kuzmany, H.; Rabolt, J. F.; Farmer, B. L.; Miller, R. D. *J. Chem. Phys.* **1986**, *85*, 7413.
(13) Lovinger, A. J.; Schilling, F. C.; Bovey, F. A.; Zeigler, J. M. *Macromolecules* **1986**, *19*, 2657.
(14) Schilling, F. C.; Lovinger, A. J.; Zeigler, J. M.; Davis, D. D.; Bovey, F. A. *Macromolecules* **1989**, *22*, 3055.
(15) Miller, R. D.; Farmers, B. L.; Fleming, W.; Sooriyakumaran, R.; Rabolt, J. F. *J. Am. Chem. Soc.* **1987**, *109*, 2509.
(16) Mintmire, J. W. *Phys. Rev. B* **1989**, *39*, 13350.
(17) Tachibana, H.; Matsumoto, M.; Tokura, Y.; Moritomo, Y.; Yamaguchi, A.; Koshihara, S.; Miller, R. D.; Abe, S. *Phys. Rev. B* **1993**, *47*, 4363.
(18) Chunwachirasiri, W.; Kanaglekar, I.; Winokur, M. J.; Koe, J. C.; West, R. *Macromolecules* **2001**, *34*, 6719.
(19) Chapman, B. R.; Farmer B. L. *Polym Prepr. (Am. Chem. Soc., Div. Polym. Chem.)* **1990**, *31*, 288.
(20) Chapman, B. R.; Patnaik, S. S.; Farmer B. L. *Polym Prepr. (Am. Chem. Soc., Div. Polym. Chem.)* **1990**, *31*, 1265.
(21) Fogarty, H. A.; Ottoson, C.-H.; Michl, J. *J. Mol. Struct. (THEOCHEM)* **2000**, *506*, 243.
(22) Fogarty, H. A.; Ottoson, C.-H.; Michl, J. *J. Mol. Struct.* **2000**, *556*, 105.
(23) Chunwachirasiri, M.; West, R.; Winokur, M. J. *Macromolecules* **2000**, *33*, 9720.
(24) Albinsson, B.; Antic, D.; Neumann, F.; Michl, J. *J. Phys. Chem. A* **1999**, *103*, 2184.
(25) Michl, J.; West, R. *Acc. Chem. Res.* **2000**, *33*, 821.
(26) Winokur, W. J.; West, R. *Macromolecules* **2003**, *36*, 7338.
(27) Furukawa, S.; Takeuchi, K.; Shimana, M. *J. Phys. Condens. Mater.* **1994**, *6*, 11007.
(28) Takeuchi, K.; Furukawa, S. *J. Phys. Condens. Mater.* **1993**, *5*, L601.
(29) Furukawa, S.; Koga, T. *J. Phys. Condens. Mater.* **1997**, *9*, L99.
(30) Natta, G.; Pino, P.; Corradini, P.; Danusso, F.; Mantica, E.; Mazzanti, G.; Moraglio, G. *J. Am. Chem. Soc.* **1955**, *77*, 1708.
(31) Natta, G. *Makromol. Chem.* **1960**, *35*, 94.
(32) Turner Jones, A. *Polym. Lett.* **1963**, *1*, 455.
(33) Petraccone, V.; Pirozzi, B.; Frasci, A.; Corradini, P. *Eur. Polym. J.* **1976**, *12*, 323.
(34) Azzurri, F.; Flores, A.; Alfonso, G. C.; Balta'Calleja, F. J. *Macromolecules* **2002**, *35*, 9069.
(35) Keller, A.; Cheng, S. Z. D. *Polymer* **1998**, *39*, 4461.
(36) Cheng, S. Z. D.; Keller, A. *Annu. Rev. Mater. Sci.* **1998**, *28*, 533.
(37) Obata, K.; Kira, M. *Chem. Commun.* **1998**, *12*, 1309.
(38) Kanai, T.; Ishibashi, H.; Hayashi, Y.; Oka, K.; Dohmaru, T.; Ogawa, T.; Furukawa, S. *Chem. Lett.* **2000**, *6*, 650.
(39) Schilling, F. C.; Bovey, F. A. Davis, D. D. Lovinger, A. J.; Macgregor, R. B., Jr.; Walsh, C. A.; Zeigler, J. M. *Macromolecules* **1989**, *22*, 4645.
(40) Walsh, C. A.; Schilling, F. C.; Lovinger, A. J.; Davis, D. D.; Bovey, F.A.; Zeigler, J. M. *Macromolecules* **1990**, *23*, 1742.
(41) Karikari, E. K.; Farmer, B. L.; Hoffman, C. L.; Rabolt, J. F. *Macromolecules* **1994**, *27*, 7185.
(42) Bukalov, S. S.; Leites, L. A.; West, R.; Asuke, T. *Macromolecules* **1996**, *29*, 907.

(43) Zhang, Q.; Tsui, O. K. C.; Du, B.; Zhang, F.; Tang, T.; He, T. *Macromolecules* **2000**, *33*, 9561.
(44) Huang, H.; Zhang, F.; Hu, Z.; Du, B.; He, T.; Lee, F. K.; Wang, Y.; Tsui, O. K. C. *Macromolecules* **2003**, *36*, 4084.
(45) Neher, D. *Adv. Mater.* **1995**, *7*, 691.
(46) Trefonas, P.; West, R. *Inorg. Synth.* **1988**, *25*, 58.
(47) Kajiyama, T.; Ohki, I.; Takahara, A. *Macromolecules* **1995**, *28*, 4768.
(48) Hu, Z.; Zhang, F.; Du, B.; Huang, H.; He, T. *Langmuir* **2003**, *19*, 9013.
(49) Cheng, S. Z. D.; Lotz, B. *Philos. Trans. R. Soc. London, A* **2003**, *361*, 517.
(50) Furuhashi, Y.; Iwata, T.; Sikorski, P.; Atkins, E.; Doi, Y. *Macromolecules* **2000**, *33*, 9423.
(51) Bermudez, M.; Leo'n, S.; Alema'n, C.; Muñoz-Guerra, S. *J. Polym. Sci., Polym. Phys. Ed.* **2000**, *38*, 41.
(52) Reneker, D. H.; Geil, P. H. *J. Appl. Phys.* **1960**, *31*, 1916.
(53) Khoury, F.; Padden, F. J., Jr. *J. Polym. Sci.* **1960**, *47*, 455.
(54) Geil, P. H. *Polymer Single Crystals*; Interscience Publishers: New York, 1963.
(55) Sauer, J. A.; Morrow, D. R.; Richardson, G. C. *J. Appl. Phys.* **1965**, *36*, 3017.
(56) Hisosaka, M. *Polymer* **1987**, *28*, 1257. Hisosaka, M. *Polymer* **1990**, *31*, 458.
(57) Guntherrodt, H.-H.; Wiesendanger, R. *Scanning Tunneling Microscopy*; Springer-Verlag: New York, 1992−1993; Vols. I−III.
(58) Shimomura, M.; Ueno, K.; Okumoto, H.; Shen, J.; Ito, K. *Macromolecules* **1994**, *27*, 7006.
(59) Shimomura, M.; Okumoto, H.; Kaito, A.; Ueno, K.; Shen, J.; Ito, K. *Macromolecules* **1998**, *31*, 7483.
(60) Jaffé, H. H.; Orchin, M. *Theory and applications of ultraviolet sepectroscopy*; John Wiley & Sons: New York, 1962.
(61) Taguchi, K.; Miyaji, H.; Izumi, K. Hoshino, A.; Miyamoto, Y.; Kokawa, R. *Polymer* **2001**, *42*, 7443.

MA034945N